AIMS Mathematics, 11(3): 6499–6524.
DOI: 10.3934/math.2026269
Received: 09 December 2025
Revised: 21 February 2026
Accepted: 04 March 2026
Published: 13 March 2026

https://www.aimspress.com/journal/Math

Research article

Two-dimensional master stability function analysis of synchronization in periodic and chaotic networks

Tayebeh Moalemi[1], Gopinath Barathi[2,3], Atiyeh Bayani[1], Karthikeyan Rajagopal[2,4], Sajad Jafari[1,5] and Matjaž Perc [6,7,8,9,*]

[1] Department of Biomedical Engineering, Amirkabir University of Technology (Tehran Polytechnic), Iran
[2] Center for Research, Easwari Engineering College, Chennai, India
[3] Center for Research, SRM TRP Engineering College, Trichy, India
[4] Center for Cognitive Science, Trichy SRM Medical College Hospital and Research Center, Trichy, India
[5] Health Technology Research Institute, Amirkabir University of Technology (Tehran Polytechnic), Iran
[6] Faculty of Natural Sciences and Mathematics, University of Maribor, Koroška cesta 160, 2000 Maribor, Slovenia
[7] Community Healthcare Center Dr. Adolf Drolc Maribor, Ulica talcev 9, 2000 Maribor, Slovenia
[8] Department of Physics, Kyung Hee University, 26 Kyungheedae-ro, Dongdaemun-gu, Seoul 02447, Republic of Korea
[9] University College, Korea University, 145 Anam-ro, Seongbuk-gu, Seoul 02841, Republic of Korea

* **Correspondence:** Email: matjaz.perc@gmail.com, matjaz.perc@um.si.

Abstract: Here we used the master stability function (MSF) framework to develop a two-dimensional MSF representation that incorporates both real and complex eigenvalues, thereby capturing the dynamics of diagonalizable directed networks. Our analysis shows how synchronization stability depends on complex coupling strengths and reveals conditions under which bounded or unbounded regions of negative MSF arise, corresponding to stable synchronization. This two-dimensional approach unifies periodic and chaotic dynamics within a common framework, offering sharper insights into when and how diagonalizable directed networks can sustain coherent collective behavior.

Keywords: master stability function; synchronization; two-dimensional analysis; chaotic systems; periodic systems
Mathematics Subject Classification: 65P20, 34D06, 05C82

1. Introduction

In nature, many systems consist of dynamical units interconnected through diverse types of links, including biological, chemical, social, neural, and technological networks such as the world wide web [1–4]. To gain insight into the underlying processes and mechanisms of such systems, researchers often construct mathematical models [5,6]. A widely used approach employs graph theory, where nodes represent dynamical units and edges represent their interactions [7]. For example, in neural systems each node may represent a neuron, while edges capture the connections between them [8,9]. In such graph-based models, interactions are typically represented by numerical values that indicate the existence and strength of coupling [10–12].

Complex networks of dynamical systems often exhibit coordinated behavior, known as synchronization, which may arise either through internal coupling or under external excitation [13,14]. Various forms of synchronization and their dynamical routes have been studied extensively, particularly in networks of chaotic oscillators [15,16]. In the case of complete synchronization, all systems evolve identically in time, sharing the same state at each moment [17,18]. In experimental sciences such as biology and sociology, synchronization underlies a broad range of phenomena [19–21]. Many essential human activities emerge from simultaneous physiological processes [22,23], and disruptions in synchronization can lead to disease or impaired function [24]. For instance, in the human brain each neuron is a dynamical unit embedded in a complex network [25]. Coordinated neuronal activity supports cognition and memory, while disturbances in synchronization are linked to disorders such as epilepsy, schizophrenia, or the perceptual impairments observed in Alzheimer's disease [26,27].

Analyzing the stability of synchronization is therefore crucial for understanding the collective behavior of networks under diverse conditions [15,28]. One of the most influential frameworks for this purpose is the master stability function (MSF), which has become a central and reliable tool for studying synchronization phenomena [29]. Its power lies in its independence from the detailed network topology: For a given dynamical system and coupling scheme, an MSF diagram can be constructed and combined with the Laplacian eigenvalues of the network to identify coupling ranges that ensure stable synchronization. The framework assumes identical oscillators, homogeneous coupling, and existence of a synchronization manifold [29]. Recent work has extended the MSF approach to account for heterogeneity by quantifying how parameter mismatches influence synchronization error through variational dynamics, and by introducing a curvature-based function that predicts the impact of structural and dynamical heterogeneity on stability [30,31].

In [32], MSF diagrams were constructed for several widely studied chaotic systems under different coupling schemes, assuming real Laplacian eigenvalues. These diagrams were classified according to the number of zero crossings of the MSF curve. However, two-dimensional MSF diagrams for chaotic systems in the presence of complex Laplacian eigenvalues have not yet been systematically explored. Complex eigenvalues naturally arise in directed networks [33], which are ubiquitous in real-world settings [34]. In many physical systems, information or energy transfer is inherently unidirectional [35]. Directed networks thus play a central role in modeling neural circuits, gene regulatory networks, and metabolic pathways [36]. Developing two-dimensional MSF diagrams,

defined over both real and imaginary axes, is therefore of considerable importance.

Recent advances in chaos-based secure communication further highlight the practical relevance of synchronization analysis in directed networks [37]. For example, recent studies on memristive and fractional-order networks further emphasize the practical importance of synchronization analysis in directed and asymmetric dynamical systems [37]. Memristive Hopfield and Cohen–Grossberg neural networks have been shown to generate hyperchaotic, multiscroll, and extreme multistable dynamics, and they have been successfully applied to secure image and video encryption in telemedicine and Industrial Internet of Things (IIoT) environments [38,39], as well as to event-triggered synchronization control under time-varying delays. In such applications, nonreciprocal couplings, delayed feedback [40], memristive autapses [41], and fractional-order [42] effects naturally lead to complex network structures with complex spectral properties. The two-dimensional master stability function framework provides a unifying theoretical tool to assess synchronization robustness in these settings by explicitly accounting for complex Laplacian eigenvalues. In particular, the identification of bounded and unbounded stability regions in the complex coupling plane offers insight into how synchronization can be maintained under reduced communication updates, hardware constraints, parameter drift, and adversarial perturbations.

Beyond the conceptual limitation, extending the MSF framework to directed networks also introduces a significant technical challenge. In the presence of complex Laplacian eigenvalues, synchronization stability must be evaluated over a two-dimensional parameter space corresponding to the real and imaginary parts of the effective coupling. This requires computing a high-resolution two-dimensional Lyapunov exponent landscape, which is computationally demanding and difficult to interpret, particularly for different node dynamics and coupling schemes. The lack of a systematic framework for constructing and analyzing such two-dimensional stability maps has hindered the practical application of MSF-based methods to directed networks.

In this paper, we used the MSF framework to construct two-dimensional MSF diagrams for a variety of chaotic systems under different coupling schemes. The chaotic systems have critical roles in electronic circuits [43], secure communication schemes [44], and biological models [45–47], where their sensitivity to initial conditions and broadband spectral characteristics are leveraged for applications such as chaos-based encryption , secure key generation, robust signal masking, and neuron modeling [48,49]. In addition, inspired by [50], which examined MSF diagrams for periodic systems, we also present two-dimensional MSF diagrams for several representative periodic systems. Finally, we provide a classification of the distinct types of two-dimensional MSF diagrams that arise in both chaotic and periodic dynamics.

The main contributions of this work are as follows:

- The master stability function framework is extended to a two-dimensional coupling domain, enabling a systematic analysis of synchronization stability in diagonalizable directed networks with complex Laplacian spectra.
- High-resolution two-dimensional MSF landscapes are computed for a broad class of node dynamics, including chaotic, forced, and periodic systems, under all single-variable diffusive coupling configurations.
- The resulting MSF diagrams are classified based on the existence of stable (negative) regions and on whether these regions are bounded or unbounded in the complex coupling plane.
- Common geometric features and qualitative trends across different dynamical regimes are identified and related to the nature of the node dynamics (chaotic versus periodic) and the role of coupling direction.
- Practical implications of the proposed framework for synchronization in directed networks are

discussed, with particular relevance to applications such as secure communication and cluster synchronization.

2. Materials and methods

A collection of interacting dynamical systems interconnected through links is referred to as a dynamical network. The structure of the network and the dynamics of its individual units jointly determine the network's collective behavior. Formally, a network consists of N nodes linked by directed or undirected edges. The presence or absence of connections is encoded in an adjacency matrix G, which serves as a mathematical representation of the network's topology. To define the elements of this matrix, nodes are first indexed, then the matrix entry G_{ij} is set to 1 if node i is connected to node j, and 0 otherwise. Consider a network of N identical d-dimensional oscillators governed by the dynamics as

$$\dot{\mathbf{x}}_i = \mathbf{F}(\mathbf{x}_i) - \sigma \sum_{j=1}^{N} L_{ij}\mathbf{H}(\mathbf{x}_j), \tag{1}$$

where $\mathbf{x}_i \in R^d$ is the state vector of node i, $\mathbf{F}$ defines the intrinsic dynamics, $\mathbf{H}$ is the coupling function, σ is the global coupling strength, and L is the Laplacian matrix of the network. The coupling function $\mathbf{H}(\mathbf{x}_j)$ specifies which components of the oscillator state participate in the network interaction. For each oscillator model, the single-variable coupling configuration $i \to j$ represents the influence of coupling from the i-th variable of the oscillators to the j-th variable. So, for three-dimensional systems, there are nine, and for two-dimensional systems, there are four single-variable coupling configurations, which are shown in Table 1.

Table 1. All nine possible coupling configurations between the state variables of 3D systems and their corresponding coupling functions, $\mathbf{H}(x, y, z)$, and Jacobian matrices $D\mathbf{H}$. Each configuration defines which variable of a node transmits its state to which variable of its neighbors in the network. The choice of coupling determines the structure of the variational equations and consequently the shape of the MSF.

Source variable	Target variable x	y	z
x	$\mathbf{H} = [x,0,0]^T$ $D\mathbf{H} = \begin{bmatrix} 1 & 0 & 0 \\ 0 & 0 & 0 \\ 0 & 0 & 0 \end{bmatrix}$	$\mathbf{H} = [0,x,0]^T$ $D\mathbf{H} = \begin{bmatrix} 0 & 0 & 0 \\ 1 & 0 & 0 \\ 0 & 0 & 0 \end{bmatrix}$	$\mathbf{H} = [0,0,x]^T$ $D\mathbf{H} = \begin{bmatrix} 0 & 0 & 0 \\ 0 & 0 & 0 \\ 1 & 0 & 0 \end{bmatrix}$
y	$\mathbf{H} = [y,0,0]^T$ $D\mathbf{H} = \begin{bmatrix} 0 & 1 & 0 \\ 0 & 0 & 0 \\ 0 & 0 & 0 \end{bmatrix}$	$\mathbf{H} = [0,y,0]^T$ $D\mathbf{H} = \begin{bmatrix} 0 & 0 & 0 \\ 0 & 1 & 0 \\ 0 & 0 & 0 \end{bmatrix}$	$\mathbf{H} = [0,0,y]^T$ $D\mathbf{H} = \begin{bmatrix} 0 & 0 & 0 \\ 0 & 0 & 0 \\ 0 & 1 & 0 \end{bmatrix}$
z	$\mathbf{H} = [z,0,0]^T$ $D\mathbf{H} = \begin{bmatrix} 0 & 0 & 1 \\ 0 & 0 & 0 \\ 0 & 0 & 0 \end{bmatrix}$	$\mathbf{H} = [0,z,0]^T$ $D\mathbf{H} = \begin{bmatrix} 0 & 0 & 0 \\ 0 & 0 & 1 \\ 0 & 0 & 0 \end{bmatrix}$	$\mathbf{H} = [0,0,z]^T$ $D\mathbf{H} = \begin{bmatrix} 0 & 0 & 0 \\ 0 & 0 & 0 \\ 0 & 0 & 1 \end{bmatrix}$

In complete synchronization, it is assumed that the oscillators in the network will all converge to a stable state, collectively forming a stable surface $\mathbf{s}(t)$. So, the difference of the variables becomes zero, and the terms related to the connections of the oscillators are eliminated, resulting in $\dot{\mathbf{s}} = \mathbf{F}(\mathbf{s})$. The

deviation from the state of complete synchronization for the oscillators is defined as $\delta\mathbf{x}_i = \mathbf{x}_i - \mathbf{s}$. The stability of synchronization in a network is equivalent to having these $\delta\mathbf{x}_i$ remain stable around the zero point. By substituting these deviations into the main equation of the network, Eq (1) can be rewritten as

$$\delta\dot{\mathbf{x}}_i = D\mathbf{F}(\mathbf{s})\delta\mathbf{x}_i - \sigma\sum_{j=1}^{N} L_{ij} D\mathbf{H}(\mathbf{s})\delta\mathbf{x}_j, \qquad i = 1, \ldots, N. \tag{2}$$

The Laplacian matrix L characterizes the coupling structure of the network, and its eigenvalues influence synchronization stability. For undirected networks, L is symmetric and thus diagonalizable with real eigenvalues. In contrast, directed or weighted asymmetric networks generally yield Laplacians with complex eigenvalues and, in some cases, non-diagonalizable structures. In connected graphs, the first eigenvalue is zero and the other eigenvalues are sorted in ascending order as $\lambda_1 = 0 < Real(\lambda_2) \leq \ldots \leq Real(\lambda_n)$. When L is diagonalizable, the system can be transformed using its eigenbasis as $\delta\boldsymbol{Y} = Q^{-1}\,\delta\,\mathbf{x}$, where Q collects the right eigenvectors of L. Noting that the Jacobian matrix $D\mathbf{F}(\boldsymbol{s})$ is block-diagonal, the main equation of the network can be expressed as N separate equations, in the form of variational equations, as

$$\delta\dot{\mathbf{Y}}_i = [D\mathbf{F}(\mathbf{s}) - \sigma\lambda_i\, D\mathbf{H}(\mathbf{s})]\delta\mathbf{Y}_i, \qquad i = 1, \ldots, N. \tag{3}$$

For non-diagonalizable Laplacians, however, the decomposition involves a Jordan form $L = PJP^{-1}$, which introduces coupling among modes within each Jordan block. Consequently, Eq (3) no longer represents fully independent equations.

For synchronization stability, it must be ensured that for all the eigenvalues, the system remains stable around zero. Considering the transformation $\xi = \delta\boldsymbol{Y}$, Eq (3) can be written as the following generic equation:

$$\dot{\xi} = [D\mathbf{F}(\mathbf{s}) - KD\mathbf{H}(\mathbf{s})]\xi, \tag{4}$$

where $K = \sigma\lambda_i$ is the complex normalized coupling strength. The largest Lyapunov exponent computed from this equation defines the master stability function, $\Psi(K)$. The stability of complete synchronization in coupled systems is investigated by computing two-dimensional MSF as a function of the complex normalized coupling strength $K = \alpha + i\beta$, where α and β denote the real and imaginary components, respectively. This generalization enables the characterization of synchronization in networks with diagonalizable directed or weighted asymmetric interactions, for which the Laplacian eigenvalues may be complex. A negative MSF indicates linear stability of the synchronous state along the corresponding transverse direction.

A variety of systems, each chosen for its relevance in physical, chemical, or biological modeling are considered. The systems analyzed include chaotic ones like Rössler, Lorenz, Hindmarsh-Rose, Chen and Chua systems; forced ones such as forced van der Pol and forced Duffing; periodic ones like Brusselator; and unforced undamped oscillators. In periodic systems, the MSF starts at zero for $K = 0$, as the largest Lyapunov exponent of an uncoupled periodic orbit is zero. This behavior contrasts with chaotic systems, where the MSF at the origin is positive. Consequently, periodic systems can exhibit synchronization behavior with more nuanced MSF profiles, including the emergence of new synchronizability classes as discussed in [50].

For each system, all coupling directions are investigated and the resulting two-dimensional MSF landscapes are classified. Also, it is examined that the negative MSF values are bounded (indicating a finite range of stable synchronization), unbounded (implying robust synchronizability), or completely absent (indicating persistent desynchronization). This comprehensive analysis enables the identification of both universal patterns and system-specific behaviors in synchronization stability

across complex coupling domains. The MSF is evaluated over a two-dimensional grid in the (α, β) plane by numerically integrating the variational equation using the MATLAB ode45 solver, which implements an explicit Runge–Kutta (4,5) method with adaptive step-size control method [51]. For each parameter pair, the synchronous trajectory is first obtained by integrating the uncoupled system over the time interval $t \in [0,4000]$, which is sufficient to eliminate transient dynamics; only the final state is retained as the initial condition for the variational equations. The combined system is then integrated in successive segments of fixed duration $T = 0.5$, after which the perturbation vector is renormalized. This procedure is repeated for $M = 15000$ iterations, corresponding to a total Lyapunov averaging time of 7500 s. The MSF is computed as the time-averaged exponential growth rate of transverse perturbations over this interval.

The Rössler system is a classical three-dimensional autonomous dynamical system introduced as a model of chaotic behavior [52]. It is often used to study fundamental properties of chaotic systems. This system is defined as

$$\begin{aligned} \dot{x} &= -y - z, \\ \dot{y} &= x + ay, \\ \dot{z} &= b + (x - \gamma)z, \end{aligned} \tag{5}$$

and its Jacobian matrix is

$$D\mathbf{F} = \begin{bmatrix} \frac{\delta \dot{x}}{\delta x} & \frac{\delta \dot{x}}{\delta y} & \frac{\delta \dot{x}}{\delta z} \\ \frac{\delta \dot{y}}{\delta x} & \frac{\delta \dot{y}}{\delta y} & \frac{\delta \dot{y}}{\delta z} \\ \frac{\delta \dot{z}}{\delta x} & \frac{\delta \dot{z}}{\delta y} & \frac{\delta \dot{z}}{\delta z} \end{bmatrix} = \begin{bmatrix} 0 & -1 & -1 \\ 1 & a & 0 \\ z & 0 & x - \gamma \end{bmatrix}, \tag{6}$$

where $a = 0.2$, $b = 0.2$, and $\gamma = 9$ yield to a chaotic response. Also, this system is analyzed when $a = 0.161$, and its response is periodic.

Originally developed to model atmospheric convection, the Lorenz system is a three-dimensional chaotic system that exhibits a well-known butterfly attractor [53]. This system is a prototypical model for exploring chaos and synchronization in physical systems. It is defined as

$$\begin{aligned} \dot{x} &= \sigma(y - x), \\ \dot{y} &= x(\rho - z) - y, \\ \dot{z} &= xy - bz, \end{aligned} \tag{7}$$

and its Jacobian matrix is

$$D\mathbf{F} = \begin{bmatrix} \frac{\delta \dot{x}}{\delta x} & \frac{\delta \dot{x}}{\delta y} & \frac{\delta \dot{x}}{\delta z} \\ \frac{\delta \dot{y}}{\delta x} & \frac{\delta \dot{y}}{\delta y} & \frac{\delta \dot{y}}{\delta z} \\ \frac{\delta \dot{z}}{\delta x} & \frac{\delta \dot{z}}{\delta y} & \frac{\delta \dot{z}}{\delta z} \end{bmatrix} = \begin{bmatrix} -\sigma & \sigma & 0 \\ \rho - z & -1 & -x \\ y & x & -b \end{bmatrix}, \tag{8}$$

when $\sigma = 10$, $\rho = 28$, and $b = 2$ yields to a chaotic attractor.

The Hindmarsh-Rose system models the membrane potential dynamics of a spiking neuron [54]. It captures both spiking and bursting behaviors, depending on parameter choices. This biologically inspired system is widely used in computational neuroscience for studying synchronization among

coupled neural oscillators. It is characterized as

$$\begin{aligned} \dot{x} &= y + 3x^2 - x^3 - z + I, \\ \dot{y} &= 1 - 5x^2 - y, \\ \dot{z} &= -rz + rs(x + 1.6), \end{aligned} \tag{9}$$

and its Jacobian matrix is

$$D\mathbf{F} = \begin{bmatrix} \frac{\delta \dot{x}}{\delta x} & \frac{\delta \dot{x}}{\delta y} & \frac{\delta \dot{x}}{\delta z} \\ \frac{\delta \dot{y}}{\delta x} & \frac{\delta \dot{y}}{\delta y} & \frac{\delta \dot{y}}{\delta z} \\ \frac{\delta \dot{z}}{\delta x} & \frac{\delta \dot{z}}{\delta y} & \frac{\delta \dot{z}}{\delta z} \end{bmatrix} = \begin{bmatrix} -3x^2 + 6x & 1 & -1 \\ -10x & -1 & 0 \\ rs & 0 & -r \end{bmatrix}, \tag{10}$$

when $I = 3.2$, $r = 0.006$, and $s = 4$ yields a chaotic response, and whereas a periodic response occurs when $r = 5.6 \times 10^{-3}$.

The Chen system is a three-dimensional chaotic oscillator similar in form to the Lorenz system but exhibiting distinct dynamical properties [52]. It is used to explore generalized synchronization behaviors and has been a benchmark in chaos theory and secure communications. This system is characterized as

$$\begin{aligned} \dot{x} &= a(y - x), \\ \dot{y} &= x(c - a - z) + cy, \\ \dot{z} &= xy - bz, \end{aligned} \tag{11}$$

and its Jacobian matrix is

$$D\mathbf{F} = \begin{bmatrix} \frac{\delta \dot{x}}{\delta x} & \frac{\delta \dot{x}}{\delta y} & \frac{\delta \dot{x}}{\delta z} \\ \frac{\delta \dot{y}}{\delta x} & \frac{\delta \dot{y}}{\delta y} & \frac{\delta \dot{y}}{\delta z} \\ \frac{\delta \dot{z}}{\delta x} & \frac{\delta \dot{z}}{\delta y} & \frac{\delta \dot{z}}{\delta z} \end{bmatrix} = \begin{bmatrix} -a & a & 0 \\ c - a - z & c & x \\ y & x & -b \end{bmatrix}, \tag{12}$$

when $a = 35$, $b = \frac{8}{3}$, and $c = 28$.

Chua's circuit is a piecewise-linear, electronic oscillator and is one of the simplest systems capable of generating chaotic attractors [52]. It is extensively used in engineering to study nonlinear circuits and chaos-based synchronization. Chua's circuit is defined as

$$\begin{aligned} \dot{x} &= a\big(y - x + f(x)\big), \\ \dot{y} &= x - y + z, \\ \dot{z} &= -by - \gamma z, \end{aligned} \tag{13}$$

and

$$f(x) = \begin{cases} -b_1 x - a_1 + b_1, & x > 1, \\ -a_1 x, & |x| < 1, \\ -b_1 x + a_1 - b_1 & x < -1, \end{cases} \tag{14}$$

and its Jacobian matrix is

$$D\mathbf{F} = \begin{bmatrix} \frac{\delta \dot{x}}{\delta x} & \frac{\delta \dot{x}}{\delta y} & \frac{\delta \dot{x}}{\delta z} \\ \frac{\delta \dot{y}}{\delta x} & \frac{\delta \dot{y}}{\delta y} & \frac{\delta \dot{y}}{\delta z} \\ \frac{\delta \dot{z}}{\delta x} & \frac{\delta \dot{z}}{\delta y} & \frac{\delta \dot{z}}{\delta z} \end{bmatrix} = \begin{bmatrix} -a - a \times \begin{cases} b_1, |x| > 1 \\ a_1, |x| < 1 \end{cases} & a & 0 \\ 1 & -1 & 1 \\ 0 & -\beta & -\gamma \end{bmatrix}, \tag{15}$$

when $a = 10,\ b = 14.87,\ a_1 = -1.27,\ b_1 = -0.68,$ and $\gamma = 0$

As mentioned, two forced systems are considered in this study. First one is the forced Duffing oscillator. This oscillator is a nonlinear second-order system driven by an external periodic force [55]. It exhibits both periodic and chaotic regimes depending on the forcing parameters and is widely used to model nonlinear mechanical vibrations and electronic systems. It is characterized as

$$\begin{aligned} \dot{x} &= y, \\ \dot{y} &= -hy - x^3 + q.\sin(\eta t), \end{aligned} \tag{16}$$

and its Jacobian matrix is

$$D\mathbf{F} = \begin{bmatrix} \frac{\delta \dot{x}}{\delta x} & \frac{\delta \dot{x}}{\delta y} \\ \frac{\delta \dot{y}}{\delta x} & \frac{\delta \dot{y}}{\delta y} \end{bmatrix} = \begin{bmatrix} 0 & 1 \\ -3x^2 & -h \end{bmatrix}, \tag{17}$$

when $\eta = 1,\ h = 0.1,$ and $q = 5.6.$

The other forced system is a forced van der Pol system. This system represents a nonlinear oscillator with both nonconservative and driven components [56]. Originally designed to model electrical circuits with vacuum tubes, the forced van der Pol oscillator displays limit cycle behavior and, under forcing, complex periodic and chaotic dynamics. It serves as a fundamental example of self-sustained oscillations in biology and electronics; it is defined as

$$\begin{aligned} \dot{x} &= y, \\ \dot{y} &= -x + d(1 - x^2)y + F.\sin(\eta t), \end{aligned} \tag{18}$$

and its Jacobian matrix is

$$D\mathbf{F} = \begin{bmatrix} \frac{\delta \dot{x}}{\delta x} & \frac{\delta \dot{x}}{\delta y} \\ \frac{\delta \dot{y}}{\delta x} & \frac{\delta \dot{y}}{\delta y} \end{bmatrix} = \begin{bmatrix} 0 & 1 \\ -1 - 2dxy & d(1 - x^2) \end{bmatrix}, \tag{19}$$

where $d = 3,\ F = 15,$ and $\eta = 4.065.$

Also, two periodic two-dimensional oscillators are considered. The first one is the Brusselator. This model is designed for autocatalytic chemical reactions. It is a canonical example of a system exhibiting limit-cycle oscillations and has been extensively studied in the context of pattern formation, chemical synchronization, and reaction-diffusion dynamics [57]. It is defined as

$$\begin{aligned} \dot{x} &= a + x^2 y - (b + 1)x, \\ \dot{y} &= bx - x^2 y, \end{aligned} \tag{20}$$

and its Jacobian matrix is

$$D\mathbf{F} = \begin{bmatrix} \frac{\delta \dot{x}}{\delta x} & \frac{\delta \dot{x}}{\delta y} \\ \frac{\delta \dot{y}}{\delta x} & \frac{\delta \dot{y}}{\delta y} \end{bmatrix} = \begin{bmatrix} 2xy - (b+1) & x^2 \\ b - 2xy & -x^2 \end{bmatrix}, \tag{21}$$

when $a = 1$ and $b = 3$.

The last periodic system is an unforced undamped Duffing oscillator. This is a conservative, two-dimensional nonlinear system that models the dynamics of a double-well potential [55]. In the absence of damping and forcing, it exhibits regular periodic motion, making it suitable for studying synchronization in purely Hamiltonian systems. This system is characterized as

$$\begin{aligned} \dot{x} &= y, \\ \dot{y} &= x - x^3, \end{aligned} \tag{22}$$

and its Jacobian matrix is

$$D\mathbf{F} = \begin{bmatrix} \frac{\delta \dot{x}}{\delta x} & \frac{\delta \dot{x}}{\delta y} \\ \frac{\delta \dot{y}}{\delta x} & \frac{\delta \dot{y}}{\delta y} \end{bmatrix} = \begin{bmatrix} 0 & 1 \\ 1 - 3x^2 & 0 \end{bmatrix}. \tag{23}$$

For each system, all coupling directions are investigated and the resulting two-dimensional MSF landscapes are classified. Also, we examine whether the negative MSF values are bounded (indicating a finite range of stable synchronization), unbounded (implying robust synchronizability), or completely absent (indicating persistent desynchronization). This comprehensive analysis enables the identification of both universal patterns and system-specific behaviors in synchronization stability across complex coupling domains.

3. Results

The two-dimensional master stability function of the Rössler system is examined as a function of the real part (α) and imaginary part (β) of the normalized coupling strength (K) in Figure 1. Regions where the MSF is negative, shown in green, indicate stable synchronization, whereas red areas correspond to desynchronized states with positive MSF values. White regions represent MSF values near zero. In each panel, the notation $i \to j$ denotes coupling from the ith component of one oscillator to the jth component of another. This notation convention and color coding are consistently used throughout Figures 2–11 as well. The analysis reveals that for coupling directions such as $x \to y$, $x \to z$, $y \to x$, $y \to z$, $z \to y$, and $z \to z$, the MSF remains positive across all coupling strengths, indicating persistent desynchronization. Conversely, coupling from $x \to x$ exhibits negative MSF values within a limited range of K, suggesting possible synchronization in that interval. In the case of $y \to y$ and $z \to x$ couplings, unbounded negative MSF regions appear, implying synchronization over a broad range of coupling strengths. The simulations were performed using parameters $a = 0.2$, $b = 0.2$, and $\gamma = 9$.

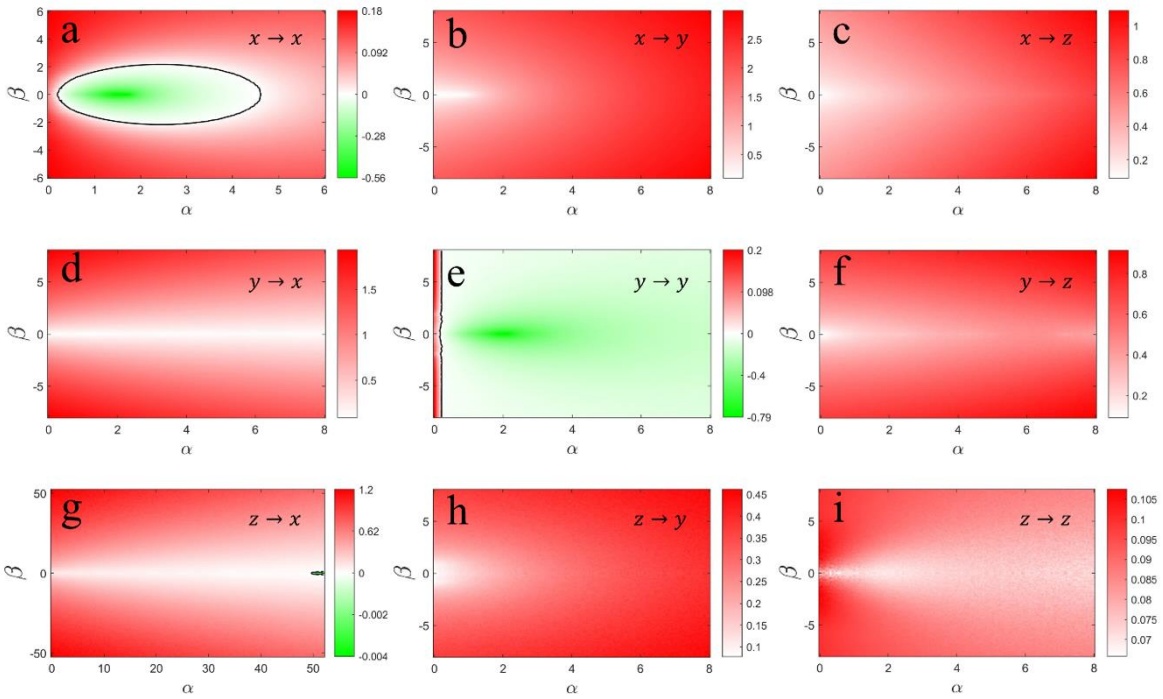

Figure 1. The two-dimensional master stability function of the Rössler system, defined in Eq (5), is shown as a function of the real (α) and imaginary (β) parts of the normalized coupling strength K when (a) $x \to x$, (b) $x \to y$, (c) $x \to z$, (d) $y \to x$, (e) $y \to y$, (f) $y \to z$, (g) $z \to x$, (h) $z \to y$, and (i) $z \to z$. The green regions indicate stable synchronization where the MSF is negative, while the red regions correspond to desynchronized regimes where the MSF is positive. White regions represent values of the MSF close to zero. In each panel, the notation $i \to j$ denotes coupling from the ith component of one oscillator to the jth component of another. This notation convention and color coding are consistently used throughout Figures 2 to 11 as well. The plot reveals that for coupling directions, such as $x \to y$, $x \to z$, $y \to x$, $y \to z$, $z \to y$, and $z \to z$, the MSF remains strictly positive, indicating desynchronization under all coupling strengths. In contrast, for $x \to x$ negative MSF values appear over a bounded interval of K, suggesting the potential for synchronization. Meanwhile, unbounded negative regions are observed for $y \to y$ and $z \to x$, implying synchronization over a broad range. The simulations use the following parameters: $a = 0.2$, $b = 0.2$, and $\gamma = 9$.

The two-dimensional master stability functions of the periodic Rössler system, defined in Eq (5), are presented as a function of the real (α) and imaginary (β) components of the normalized complex coupling strength $K = \alpha + i\beta$. The analysis of the coupling directions reveals that for $x \to y$, $x \to z$, $y \to x$, $y \to z$, $z \to y$, and $z \to z$, the MSF remains strictly positive throughout the coupling parameter space, indicating that synchronization is not supported under these configurations. Conversely, in the $x \to x$ case, negative MSF values emerge within a finite, bounded region of K, suggesting the presence of a limited synchronization window. Furthermore, for $y \to y$ and $z \to x$, the MSF exhibits extensive unbounded negative regions, implying that synchronization is attainable over a wide range of coupling strengths. The simulations are performed using parameter values $a = 0.161$, $b = 0.2$, and $\gamma = 9$.

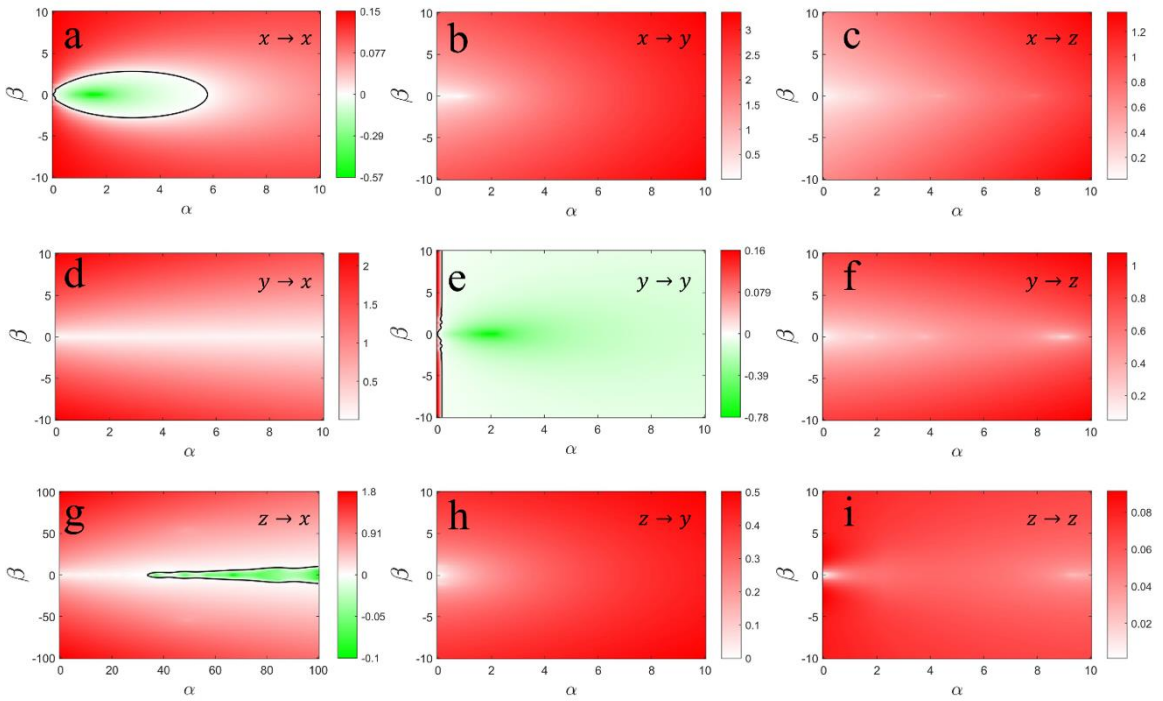

Figure 2. The two-dimensional master stability functions of the periodic Rössler system, defined in Eq (5), is shown as a function of the real (α) and imaginary (β) parts of the normalized coupling strength K when (a) $x \to x$, (b) $x \to y$, (c) $x \to z$, (d) $y \to x$, (e) $y \to y$, (f) $y \to z$, (g) $z \to x$, (h) $z \to y$, and (i) $z \to z$. For coupling directions including $x \to y$, $x \to z$, $y \to x$, $y \to z$, $z \to y$, and $z \to z$, the MSF values remain consistently positive, indicating desynchronization across all coupling strengths. In contrast, for the $x \to x$ direction, negative MSF values emerge within a bounded interval of K, suggesting the potential for synchronization under those conditions. Meanwhile, unbounded negative regions are observed for $y \to y$ and $z \to x$, implying robust synchronization over a broad parameter range. The simulations were conducted using the parameters: $a = 0.161$, $b = 0.2$, and $\gamma = 9$.

A comparison between Figures 1 and 2 indicates that the overall synchronization properties of the chaotic and periodic Rössler systems are qualitatively similar, with the same coupling directions admitting bounded or unbounded regions of negative MSF and others remaining strictly unstable. In particular, the coupling configurations that support stable synchronization and those that lead to desynchronization are preserved across both dynamical regimes. The primary distinction lies in the location of the stability regions in the complex coupling plane. For the periodic Rössler system (Figure 2), the onset of stable synchronization occurs from the vicinity of $\alpha = 0$ and $\beta = 0$, with negative MSF values emerging near the origin and extending outward depending on the coupling direction. In contrast, in the chaotic regime (Figure 1), stable synchronization regions do not necessarily originate at the origin and may appear at finite values of the coupling parameters. This observation indicates that while the existence and type of synchronization regimes remain unchanged, the periodic dynamics favor synchronization that initiates from weak coupling, whereas chaotic dynamics require finite coupling to achieve stability.

The two-dimensional MSF for the Lorenz system, defined in Eq (6), is depicted as a function of

the normalized coupling strength components α and β. The graph shows that for coupling directions such as $x \to z$, $y \to z$, $z \to x$, and $z \to y$, the MSF remains strictly positive, indicating persistent desynchronization regardless of the coupling strength. Conversely, for coupling direction $y \to x$, the MSF attains negative values within bounded intervals of the coupling parameter K, suggesting possible synchronization in these ranges. Additionally, unbounded regions of negative MSF are found for $x \to x$, $x \to y$, and $y \to y$ directions, indicating that synchronization can occur over an extensive range of coupling strengths. Also, for $z \to z$ direction, the MSF displays a bounded region of negative values together with an unbounded negative region, indicating the existence of locally and globally robust synchronization regimes. The simulations were conducted with parameters $\sigma = 10$, $\rho = 28$, and $b = 2$.

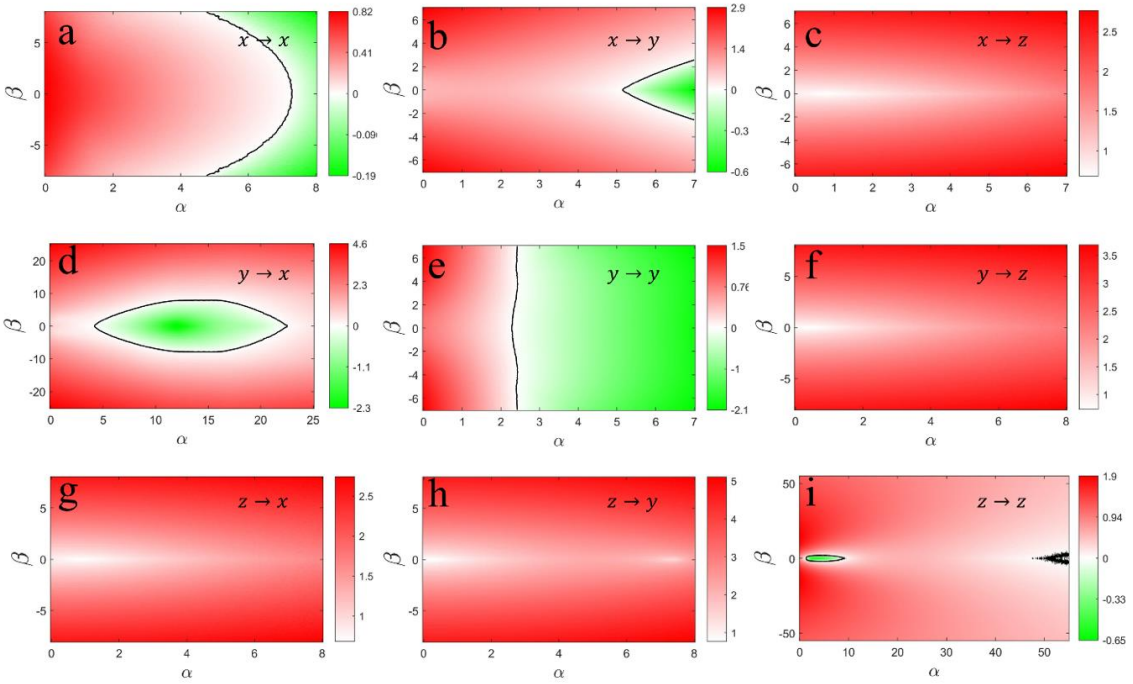

Figure 3. The two-dimensional master stability function of the Lorenz system, defined in Eq (6), is shown as a function of α and β parts of the normalized coupling strength when (a) $x \to x$, (b) $x \to y$, (c) $x \to z$, (d) $y \to x$, (e) $y \to y$, (f) $y \to z$, (g) $z \to x$, (h) $z \to y$, and (i) $z \to z$. The analysis of the plot demonstrates that for coupling configurations such as $x \to z, y \to z, z \to x$, and $z \to y$, the MSF consistently maintains positive values, signifying desynchronization across all coupling strengths. Conversely, for $y \to x$, negative MSF values emerge within distinct finite ranges of K, indicating a possibility for synchronization in these intervals. Notably, unbounded negative regions are evident for $x \to x, x \to y$, and $y \to y$, suggesting robust synchronization across a wide parameter space. Also, for the $z \to z$ direction, the MSF displays a bounded region of negative values together with an unbounded negative region, indicating the existence of locally and globally robust synchronization regimes. The simulations were conducted using the parameters: $\sigma = 10, \rho = 28,$ and $b = 2$.

The two-dimensional master stability function of the Hindmarsh-Rose neuronal system, defined in Eq (7), is illustrated as a function of the normalized coupling strength components α and β. The

analysis of the MSF reveals that for coupling directions like $x \rightarrow z$, $y \rightarrow z$, $z \rightarrow x$, $z \rightarrow y$, and $z \rightarrow z$, the MSF remains strictly positive, signaling persistent desynchronization regardless of the coupling strength applied. This indicates that such coupling pathways are ineffective at promoting synchronized behavior in the system over any range of coupling intensities. In contrast, the $y \rightarrow x$ coupling direction exhibits negative MSF values over bounded interval of the coupling parameter K, suggesting windows where synchronization can emerge. This behavior points to the possibility of tuning coupling strength to achieve synchronization selectively in this direction. Moreover, for the directions $x \rightarrow x$, $x \rightarrow y$, and $y \rightarrow y$, the MSF attains unbounded negative values over broad regions, indicating a robust propensity for synchronization across an extensive range of coupling strengths. Such unbounded negative regions imply that once synchronized, the system can maintain stable synchrony even with variations in coupling intensity, highlighting these directions as particularly effective for controlling synchronized dynamics. The investigation employs the parameter set $I = 3.2$, $r = 0.006$, and $s = 4$, which are standard in modeling the Hindmarsh-Rose neuron dynamics and influence the system's intrinsic behavior and response to coupling.

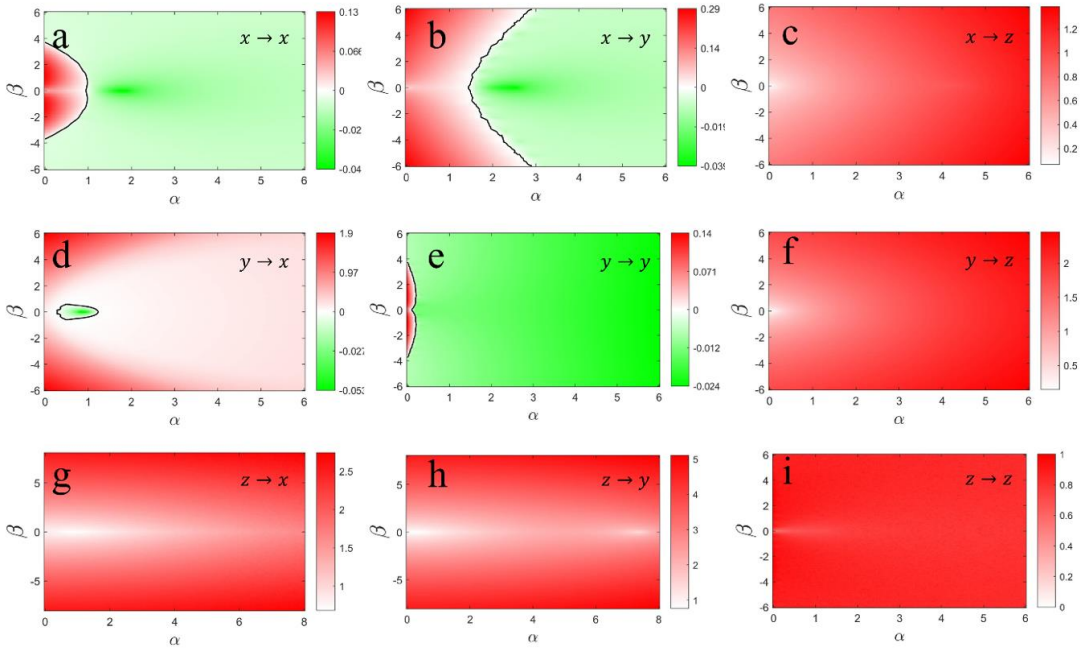

Figure 4. The two-dimensional MSF of the Hindmarsh-Rose system, defined in Eq (7), is shown as a function of α and β parts of K when (a) $x \rightarrow x$, (b) $x \rightarrow y$, (c) $x \rightarrow z$, (d) $y \rightarrow x$, (e) $y \rightarrow y$, (f) $y \rightarrow z$, (g) $z \rightarrow x$, (h) $z \rightarrow y$ and (i) $z \rightarrow z$. The analysis indicates that for coupling directions such $as\ x \rightarrow z, y \rightarrow z, z \rightarrow x, z \rightarrow y$, and $z \rightarrow z$, the MSF consistently remains positive, reflecting desynchronization across all coupling strengths. Conversely, for the $y \rightarrow x$ direction, negative MSF values emerge within bounded interval of K, hinting at the potential for synchronization in these regions. Additionally, unbounded negative regions are observed for $x \rightarrow x, x \rightarrow y$, and $y \rightarrow y$, suggesting robust synchronization over a wide range of parameters. The simulations were performed using the parameters: $I = 3.2$, $r = 0.006$, and $s = 4$.

Figure 5 illustrates the two-dimensional MSFs of the periodic Hindmarsh-Rose system, plotted with respect to the complex normalized coupling strength $K = \alpha + i\beta$. The results reveal distinct

synchronization characteristics depending on the direction of coupling. Specifically, in the cases of $x \to z$, $y \to z$, and $z \to x$, the MSF values remain strictly positive across the entire range of K, indicating a complete lack of synchronization. In contrast, for couplings such as $y \to x$, $z \to y$, and $z \to z$, the MSF becomes negative within well-defined, bounded regions of the complex plane, suggesting limited yet possible synchronization. Additionally, unbounded negative MSF regions are observed for $x \to x$, $x \to y$, and $y \to y$, indicating robust synchronization potential over a broad range of coupling strengths. These observations are based on simulations conducted with the parameters $I = 3.2$, $r = 5.6 \times 10^{-3}$, and $s = 4$.

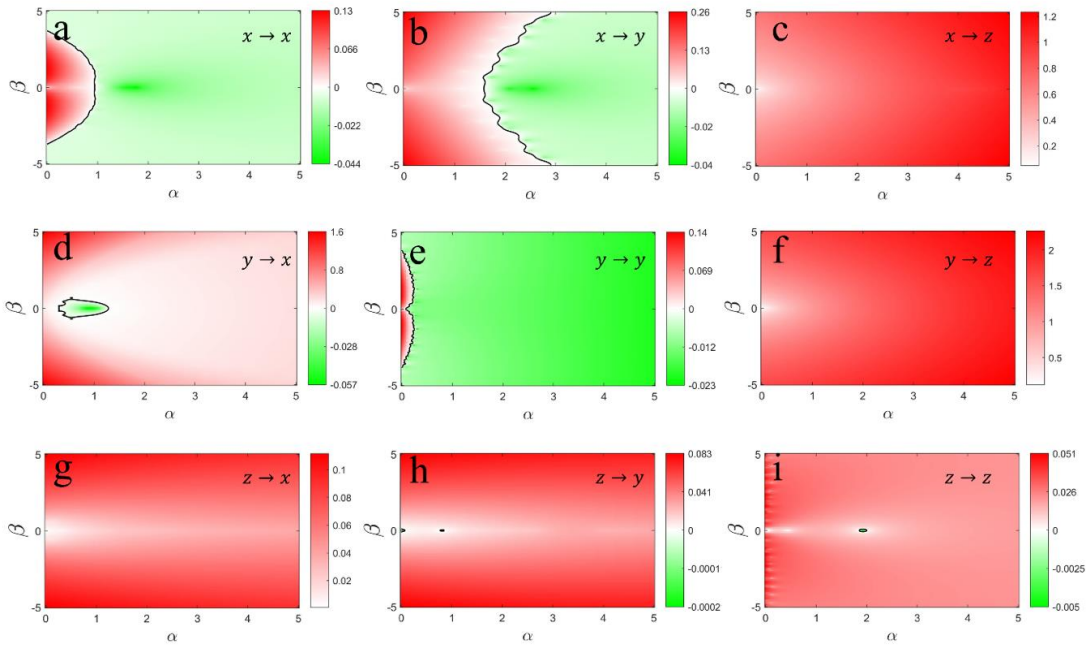

Figure 5. The two-dimensional master stability functions of the periodic Hindmarsh-Rose system are shown as a function of the complex normalized coupling strength $K = \alpha + i\beta$ when (a) $x \to x$, (b) $x \to y$, (c) $x \to z$, (d) $y \to x$, (e) $y \to y$, (f) $y \to z$, (g) $z \to x$, (h) $z \to y$ and (i) $z \to z$. The analysis indicates that for coupling directions such as $x \to z$, $y \to z$, and $z \to x$, the MSFs consistently maintain positive values, signifying desynchronization across all coupling strengths. Conversely, for $y \to x, z \to y$, and $z \to z$, negative MSF values emerge within bounded intervals of K, pointing to a potential for synchronization in these cases. Notably, unbounded negative regions are observed for $x \to x, x \to y$, and $y \to y$, suggesting robust synchronization over a wide parameter range. The simulations were performed using the parameters: $I = 3.2$, $r = 5.6 \times 10^{-3}$, and $s = 4$.

A comparison between Figures 4 and 5 reveals that, unlike the Rössler system, the synchronization response of the Hindmarsh–Rose model exhibits a stronger dependence on the underlying dynamical regime. While both chaotic and periodic HR dynamics admit unbounded negative MSF regions for the $x \to x$, $x \to y$, and $y \to y$ coupling directions, the remaining coupling configurations display qualitatively different stability structures. In the chaotic regime (Figure 4), several coupling directions such as $z \to y$ and $z \to z$, remain strictly unstable, whereas in the periodic regime (Figure 5) these directions give rise to bounded regions of negative MSF, indicating

the emergence of synchronization windows that are absent in the chaotic case. Moreover, bounded stability regions observed for $y \to x$ in the chaotic regime shift or disappear in the periodic dynamics, reflecting a reorganization of stability boundaries in the complex coupling plane. These differences indicate that, for the Hindmarsh–Rose system, periodic dynamics substantially alter both the extent and distribution of stable synchronization regions, highlighting a greater sensitivity to the intrinsic oscillatory behavior compared to the Rössler system.

The two-dimensional master stability function for Chen's system, described in Eq (8), is presented as a function of the α and β components of the normalized coupling strength (K). The graphical representation demonstrates that coupling directions such as $x \to x$, $x \to z$, $y \to x$, $y \to z$, $z \to x$, and $z \to y$ yield strictly positive MSF values, which implies that these coupling do not promote synchronization and the system remains desynchronized regardless of coupling strength. Conversely, the coupling direction $z \to z$ exhibits negative MSF values within bounded interval of the coupling parameter K, indicating the possibility of achieving synchronization in these specific ranges. Additionally, extended regions of unbounded negative MSF occur for the $x \to y$ and $y \to y$ coupling directions, suggesting that synchronization can be sustained over a wide spectrum of coupling strengths. The simulations were carried out using system parameters $a = 35$, $b = \frac{8}{3}$, and $c = 28$, which characterize the intrinsic dynamics of Chen's system and influence its synchronizability.

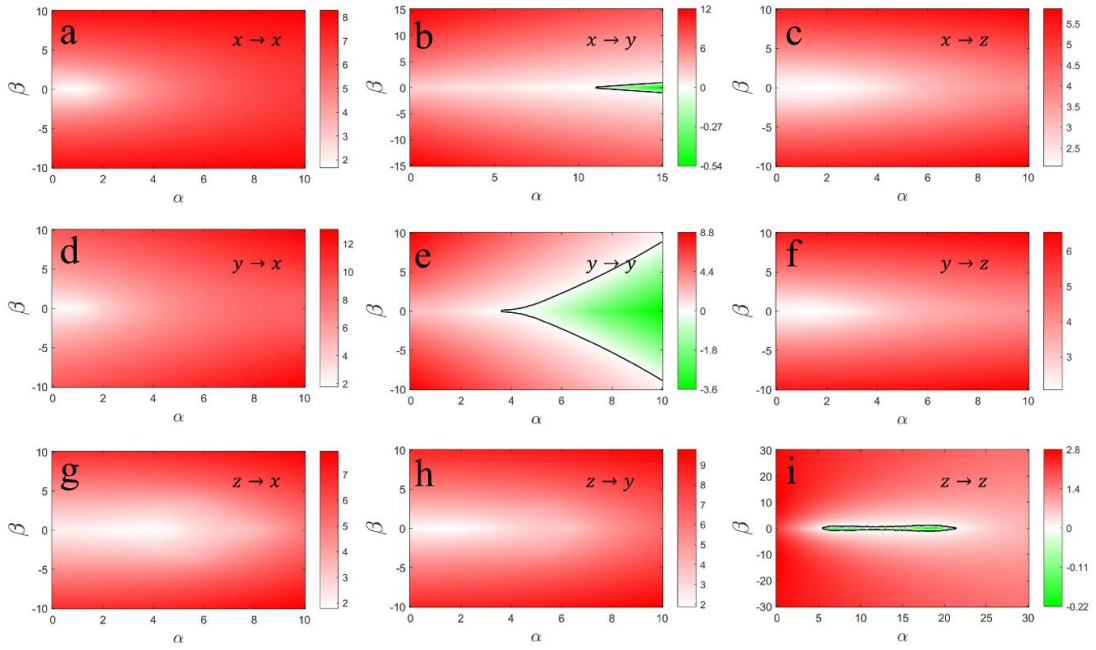

Figure 6. The two-dimensional MSF of the Chen's system, defined in Eq (8), is shown as a function of the α and β parts of the normalized coupling strength K when (a) $x \to x$, (b) $x \to y$, (c) $x \to z$, (d) $y \to x$, (e) $y \to y$, (f) $y \to z$, (g) $z \to x$, (h) $z \to y$ and (i) $z \to z$. The plot demonstrates that for coupling directions such as $x \to x, x \to z, y \to x, y \to z, z \to x$, and $z \to y$, the MSF consistently maintains positive values, indicating desynchronization across all coupling strengths. In contrast, for the $z \to z$ direction, negative MSF values emerge within bounded interval of K, suggesting the potential for synchronization in these regions. Notably, unbounded negative regions are observed for $x \to y$ and $y \to y$, implying robust synchronization over a broad parameter range. The simulations were conducted using the parameters: $a = 35$, $b = 8/3$, and $c = 28$.

The two-dimensional MSF of the Chua's circuit system, defined in Eq (9), is presented as a function of the parameters α and β. The analysis shows that for coupling directions such as $x \to z$ and $z \to y$, the MSF remains strictly positive, indicating that desynchronization occurs at all coupling strengths. Conversely, for the coupling directions $z \to x$ and $z \to z$, negative MSF values emerge over specific bounded intervals of the coupling strength K, suggesting the possibility of synchronization in these ranges. Additionally, unbounded negative MSF regions are observed for coupling directions $x \to x$, $x \to y$, $y \to x$, $y \to y$, and $y \to z$, which implies synchronization can occur across a wide range of coupling strengths. The simulations were conducted using the parameters $a = 10$, $b = 14.87$, and $\gamma = 0$.

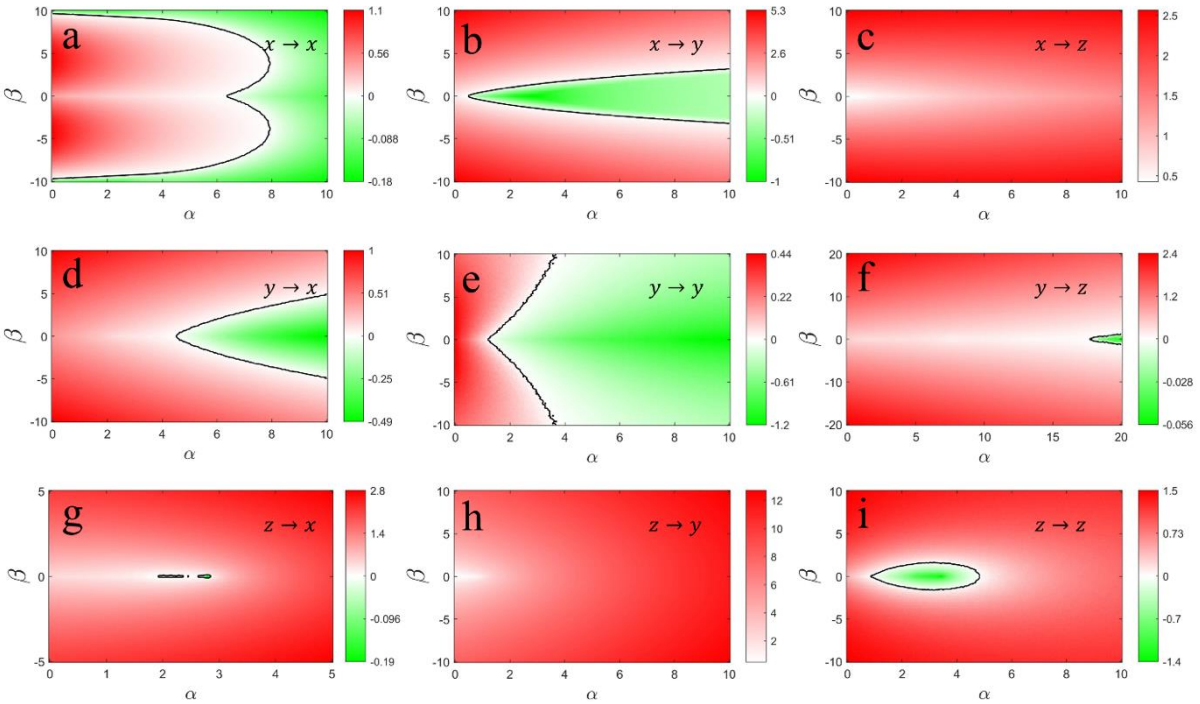

Figure 7. The two-dimensional master stability function of the Chua's circuit system, defined in Eq (9), is shown as a function of α and β when (a) $x \to x$, (b) $x \to y$, (c) $x \to z$, (d) $y \to x$, (e) $y \to y$, (f) $y \to z$, (g) $z \to x$, (h) $z \to y$ and (i) $z \to z$. The analysis shows that for coupling directions such as $x \to z$ and $z \to y$, the MSF remains consistently positive, reflecting desynchronization across all coupling strengths. Conversely, for $z \to x$ and $z \to z$, negative MSF values emerge within bounded intervals of K, indicating a potential for synchronization in these cases. Additionally, unbounded negative regions are observed for $x \to x$, $x \to y$, $y \to x$, $y \to y$, and $y \to z$, suggesting robust synchronization over a wide parameter range. The simulations were performed using the parameters: $a = 10$, $b = 14.87$, and $\gamma = 0$.

The forced Duffing oscillator is a two-dimensional dynamical system, defined in Eq (11), and its two-dimensional MSF is depicted as a function of the parameters α and β in Figure 8. For the coupling $y \to x$, negative MSF values occur within specific bounded interval of K, indicating potential synchronization. Unbounded negative MSF regions, implying synchronization over a broad range, are found for couplings $x \to x$ and $y \to y$. The coupling $x \to y$ exhibits both bounded and

unbounded negative MSF regions, suggesting a mixed synchronization behavior. The simulations were carried out with parameters $\eta = 1,\ h = 0.1$, and $q = 5.6$.

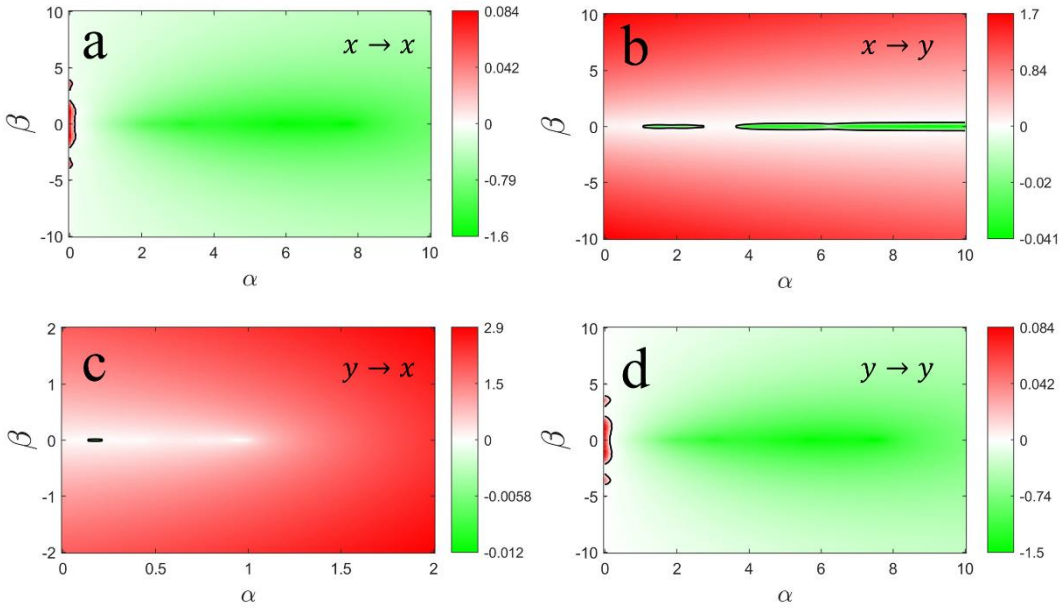

Figure 8. two-dimensional MSF of the forced Duffing oscillator, Eq (11), is shown as a function of α and β parts of K when (a) $x \to x$, (b) $x \to y$, (c) $y \to x$, and (d) $y \to y$. For the $y \to x$ coupling direction, negative MSF values emerge within bounded interval of K, indicating a potential for synchronization under certain conditions. In contrast, unbounded negative regions are observed for $x \to x$ and $y \to y$, suggesting robust synchronization across a wide range of parameters. The $x \to y$ coupling exhibits a mixed behavior, with both bounded and unbounded regions of negative MSF values, reflecting a more complex synchronization dynamic. The simulations were conducted using the parameters: $\eta = 1,\ h = 0.1,$ and $q = 5.6$.

Figure 9 presents the two-dimensional master stability functions for the Forced van der Pol system, defined in Eq (12). The MSFs are plotted as a function of the complex normalized coupling strength $K = \alpha + i\beta$. Notably, when the coupling is directed from y to x, negative MSF values, indicative of potential synchronization, emerge only within two distinct and bounded regions of the complex coupling space. In contrast, for the coupling configurations $x \to x$, $x \to y$, and $y \to y$, the MSF exhibits extensive unbounded regions of negativity, suggesting that synchronization is achievable over a wide range of coupling strengths. These results are obtained using parameter values $d = 3,\ F = 15,$ and $\eta = 4.065$.

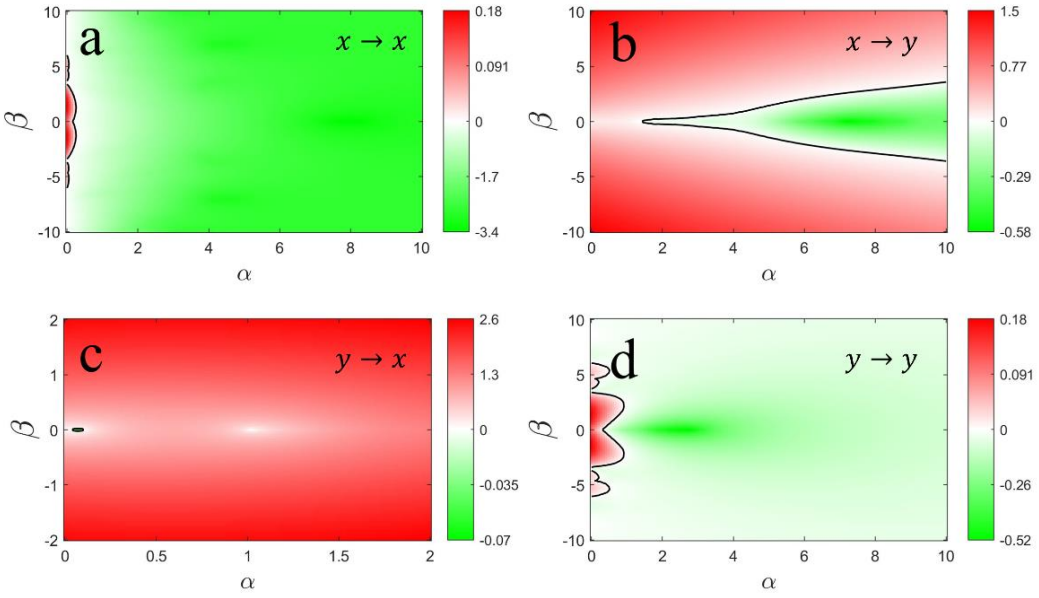

Figure 9. The two-dimensional MSF of the forced van der Pol system**,** defined in Eq (12), is shown as a function of the normalized coupling strength $K = \alpha + i\beta$ when (a) $x \to x$, (b) $x \to y$, (c) $y \to x$, and (d) $y \to y$. The plot reveals that for coupling $y \to x$ negative MSF values appear over two isolated bounded intervals of K, suggesting the potential for synchronization. Meanwhile, unbounded negative regions are observed for $x \to x, x \to y,$ and $y \to y$, implying synchronization over a broad range. The simulations use the following parameters: $d = 3, F = 15,$ and $\eta = 4.065$.

Figure 10 displays the two-dimensional MSFs of the periodic Brusselator system, defined in Eq (13), plotted with respect to the real and imaginary components of the normalized complex coupling strength $K = \alpha + i\beta$. The Brusselator is a two-dimensional reaction-diffusion model that exhibits periodic oscillations under suitable parameter choices. As expected for periodically driven systems, the MSF initiates from zero when the coupling strength is zero, reflecting the neutral stability of the uncoupled periodic orbit. The analysis reveals that for the coupling directions $y \to x$ and $y \to y$, negative MSF values emerge over bounded intervals of K, indicating the potential for synchronization under limited conditions. In contrast, the directions $x \to x$ and $x \to y$ yield unbounded regions with negative MSF values, implying that synchronization can be achieved over a broad range of coupling strengths. All simulations are carried out using the parameter values $a = 1$ and $b = 3$.

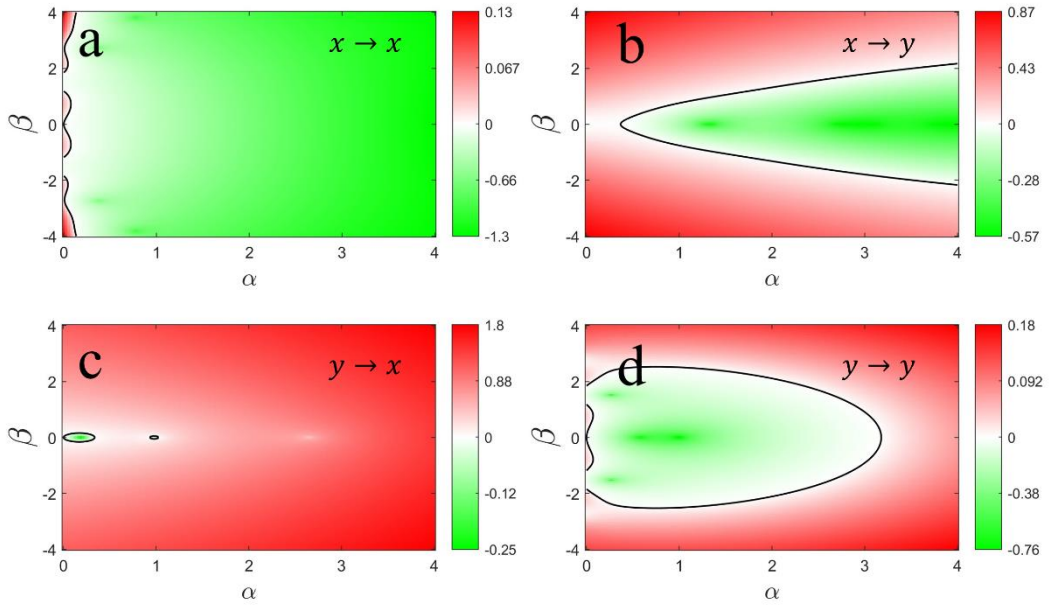

Figure 10. The two-dimensional MSFs of the periodic Brusselator, defined in Eq (13), is shown as a function of α and β parts of the normalized coupling strength K when (a) $x \to x$, (b) $x \to y$, (c) $y \to x$, and (d) $y \to y$. The plot indicates that for coupling directions $y \to x$ and $y \to y$, negative MSF values emerge within bounded intervals of K, hinting at the potential for synchronization under these conditions. Conversely, unbounded negative regions are observed for $x \to x$ and $x \to y$, suggesting robust synchronization across a wide parameter range. The simulations were performed using the parameters: $a = 1$ and $b = 3$.

Figure 11 presents the two-dimensional master stability functions of the unforced, undamped Duffing system, defined in Eq (14), plotted with respect to the real and imaginary components of the normalized complex coupling strength. This system is two-dimensional and exhibits periodic oscillatory behavior. Consistent with the properties of periodic systems, the MSF originates at zero when the coupling strength is zero, reflecting the marginal stability of the uncoupled periodic orbit. The MSF analysis reveals that for the coupling directions $x \to y$ and $y \to x$, the function remains strictly positive across the entire coupling domain, indicating the absence of synchronization regardless of the coupling strength. In contrast, the directions $x \to x$ and $y \to y$ produce a combination of both bounded and unbounded regions where the MSF assumes negative values, suggesting the existence of coupling regimes that support synchronization.

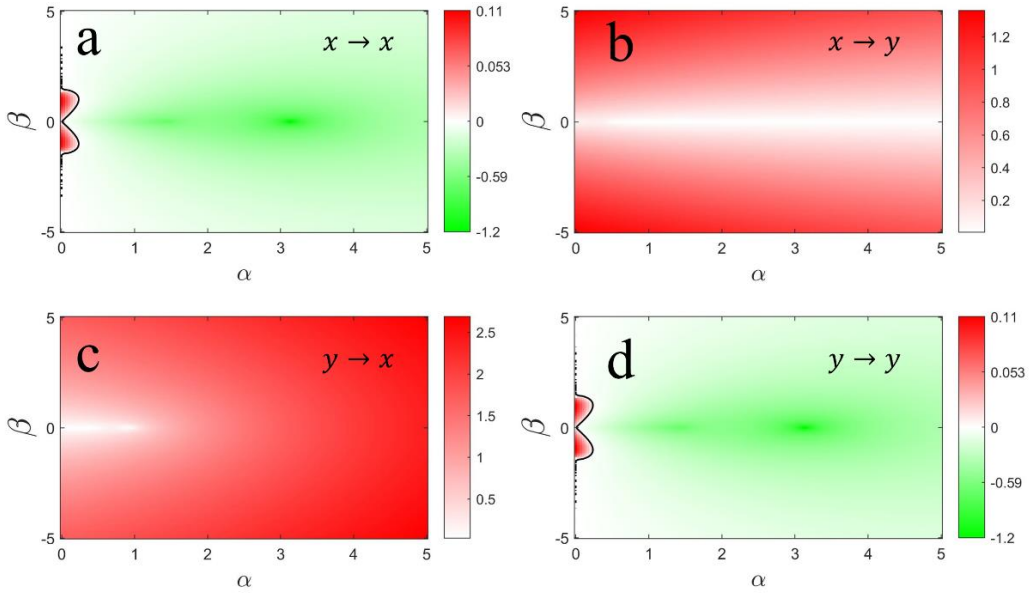

Figure 11. The two-dimensional master stability function of the unforced undamped Duffing, defined in Eq (14), is shown as a function of the real and imaginary parts of the normalized coupling strength when (a) $x \to x$, (b) $x \to y$, (c) $y \to x$, and (d) $y \to y$. For the coupling directions $x \to y$ and $y \to x$, the MSF values remain consistently positive, indicating desynchronization across all coupling strengths. In contrast, the $x \to x$ and $y \to y$ couplings display a mixed behavior, with both bounded and unbounded regions of negative MSF values, pointing to a complex interplay between synchronization and desynchronization dynamics.

4. Discussion

For diagonalizable directed networks of arbitrary size, the computational effort is governed primarily by the evaluation of the two-dimensional MSF over the relevant region of the complex plane. Once this surface is computed, the stability of synchronization for any larger network reduces to checking whether its Laplacian eigenvalues lie within the stable region. Importantly, the MSF computation itself is highly parallelizable and does not scale with the network size, while extracting the spectrum of the Laplacian depends only on standard eigenvalue routines. As a result, the method extends naturally to networks with hundreds or thousands of nodes, provided that the Laplacian is diagonalizable.

The analysis developed in this work relies on the classical assumption of identical oscillators with uniform coupling functions, which ensures the existence of a well-defined synchronization manifold, whose stability is assessed using the MSF framework. Under these conditions, perturbations transverse to the manifold evolve according to the variational equation on which the MSF is based. If oscillator parameters differ or if the coupling functions are nonuniform, this invariant manifold generally breaks down, and the MSF formalism no longer provides a complete description of the stability. By clearly outlining these assumptions, we emphasize the regime in which the present results are valid while also indicating natural directions for future generalizations.

From an application perspective, the two-dimensional MSF landscapes obtained in this work can serve as design maps for directed networked systems in which synchronization plays a functional role

rather than being an incidental phenomenon. In particular, unbounded negative MSF regions suggest coupling configurations that are inherently robust to parameter drift, sparse updates, or hardware-induced perturbations, whereas bounded stability regions point to regimes requiring careful tuning. This distinction is especially relevant for secure communication and IIoT scenarios, where synchronization must be preserved under limited communication, reduced computational overhead, and potential external interference.

The proposed two-dimensional MSF framework can be positioned relative to several foundational and representative works in the literature. In the original formulation of the MSF by Pecora and Carroll [29], the general formalism was introduced and the possibility of complex effective coupling parameters was already recognized. However, subsequent applications have largely focused on one-dimensional MSF. In contrast, the present study systematically explores the full two-dimensional MSF over the complex coupling plane for a broad class of node dynamics and for all single-variable diffusive coupling configurations, with an explicit emphasis on diagonalizable directed networks and on the distinction between bounded and unbounded stability regions.

A related line of research was presented by Huang et al. [32], where MSFs were classified according to the number of zero crossings along the real coupling axis. While this classification provides valuable insights for undirected or effectively real-coupled systems, it does not capture stability features arising from complex Laplacian eigenvalues. The present work generalizes this classification from a one-dimensional real domain to the full complex plane, incorporates both chaotic and periodic dynamics within a unified two-dimensional framework, and systematically addresses the role of complex Laplacian spectra characteristic of directed networks.

The comparison between the chaotic and periodic regimes of the Hindmarsh–Rose system reveals a markedly stronger sensitivity of synchronization properties to the underlying neuronal dynamics than observed for the Rössler system. While both regimes admit unbounded regions of negative MSF for certain self- and cross-coupling configurations, the periodic dynamics substantially reorganize the stability landscape by introducing bounded synchronization windows in coupling directions that remain strictly unstable in the chaotic case. This behavior suggests that the slow–fast structure and bursting characteristics of the Hindmarsh–Rose model play a decisive role in shaping transverse stability, particularly by modifying how perturbations evolve under weak and moderate coupling. Unlike the Rössler system, where the transition from chaotic to periodic dynamics primarily shifts the location of stability regions without altering their qualitative structure, the Hindmarsh–Rose system exhibits regime-dependent changes in both the extent and connectivity of negative MSF regions.

5. Conclusions

In summary, our investigation of two-dimensional master stability function (MSF) diagrams provides new insights into synchronization across a range of dynamical systems. We find that the Rössler and Lorenz systems are capable of achieving synchronization under specific coupling configurations, characterized by unbounded negative regions in their MSF. By contrast, the Hindmarsh–Rose and Chen systems display more limited synchronization, confined to finite parameter intervals. Importantly, the analysis highlights systematic differences between chaotic and periodic systems, with periodic dynamics exhibiting more intricate and finely structured MSF profiles.

These findings emphasize the crucial role of both coupling strength and direction in determining the stability of synchronization in complex networks. Beyond their immediate relevance to canonical dynamical systems, the results provide a framework for understanding synchronization in diagonalizable directed networks, where complex Laplacian eigenvalues naturally arise. The two-

dimensional MSF approach thus establishes a foundation for using stability analysis to broader classes of networks, including those displaying cluster synchronization and other forms of coordinated dynamics [58,59].

Author contributions

Tayebeh Moalemi: Conceptualization, formal analysis, investigation, methodology, visualization, writing–original draft, writing–review & editing; Gopinath Barathi: Conceptualization, formal analysis, investigation, methodology, visualization, writing–original draft, writing–review & editing; Atiyeh Bayani: Conceptualization, formal analysis, funding acquisition, investigation, methodology, resources, software, validation, visualization, writing–original draft, writing–review & editing; Karthikeyan Rajagopal: Formal analysis, funding acquisition, investigation, methodology, resources, writing–original draft, writing–review & editing; Sajad Jafari: Conceptualization, formal analysis, funding acquisition, investigation, methodology, project administration, resources, supervision, validation, writing–original draft, writing–review & editing; Matjaž Perc: Conceptualization, funding acquisition, project administration, resources, supervision, writing–original draft, writing–review & editing. All authors have read and approved the final version of the manuscript for publication.

Use of Generative-AI tools declaration

The authors declare they have not used Artificial Intelligence (AI) tools in the creation of this article.

Acknowledgments

Matjaž Perc was supported by the Slovenian Research and Innovation Agency (Grant No. P1-0403).

Conflict of interest

The authors declare that they have no conflict of interest.

References

1. Y. Dong, L. Huo, M. Perc, S. Boccaletti, Adaptive rumor propagation and activity contagion in higher-order networks, *Commun. Phys.*, **8** (2025), 261. https://doi.org/10.1038/s42005-025-02181-3
2. S. Boccaletti, V. Latora, Y. Moreno, M. Chavez, D. U. Hwang, Complex networks: Structure and dynamics, *Phys. Rep.*, **424** (2006), 175–308. https://doi.org/10.1016/j.physrep.2005.10.009
3. E. Agliari, A. Annibale, A. Barra, A. C. C. Coolen, D. Tantari, Immune networks: multi-tasking capabilities at medium load, *J. Phys. A-Math. Theor.*, **46** (2013), 335101. https://doi.org/10.1088/1751-8113/46/33/335101
4. E. Agliari, A. Annibale, A. Barra, A. C. C. Coolen, D. Tantari, Immune networks: Multitasking capabilities near saturation, *J. Phys. A-Math. Theor.*, **46** (2013), 415003. https://doi.org/10.1088/1751-8113/46/41/415003
5. C. M. Legaard, T. Schranz, G. Schweiger, J. Drgoňa, B. Falay, C. Gomes, et al., Constructing neural network based models for simulating dynamical systems, *ACM Comput. Surv.*, **55** (2023), 236. https://doi.org/10.1145/3567591

6. Y. J. Ma, Z. Q. Jiang, F. S. Fang, M. Perc, S. Boccaletti, Social norms and cooperation in higher-order networks, *P. Roy. Soc. A*, **480** (2024), 20240066. https://doi.org/10.1098/rspa.2024.0066
7. D. Ghosh, M. Frasca, A. Rizzo, S. Majhi, S. Rakshit, K. A. Bittner, et al., The synchronized dynamics of time-varying networks, *Phys. Rep.*, **949** (2022), 1–63. https://doi.org/10.1016/j.physrep.2021.10.006
8. S. Dang, A. Bayani, H. Tian, Z. Wang, F. Parastesh, F. Nazarimehr, et al., Investigating the route to synchronization in real-world neuronal networks of autaptic photosensitive neurons, *Chaos Soliton. Fract.*, **186** (2024), 115225. https://doi.org/10.1016/j.chaos.2024.115225
9. X. Chen, N. Wang, K. Wang, M. Chen, F. Parastesh, Q. Xu, Coupling dynamics in an FHN bi-neuron model coupled via ReLU function-based locally active memristor, *Nonlinear Dynam.*, **112** (2024), 20365–20379. https://doi.org/10.1007/s11071-024-10127-7
10. E. Bolhasani, M. Hassanzadeh, M. Perc, A. Valizadeh, Functional modularity induced by delayed interactions, *Chaos Soliton. Fract.*, **198** (2025), 116511. https://doi.org/10.1016/j.chaos.2025.116511
11. M. S. Anwar, G. K. Sar, M. Perc, D. Ghosh, Collective dynamics of swarmalators with higher-order interactions, *Commun. Phys.*, **7** (2024), 59. https://doi.org/10.1038/s42005-024-01556-2
12. S. Majhi, M. Perc, D. Ghosh, Dynamics on higher-order networks: a review, *J. Roy. Soc. Interface*, **19** (2022), 20220043. https://doi.org/10.1098/rsif.2022.0043
13. I. Franović, K. Todorović, N. Vasović, N. Burić, Stability, coherent spiking and synchronization in noisy excitable systems with coupling and internal delays, *Commun. Nonlinear Sci.*, **19** (2014), 3202–3219. https://doi.org/10.1016/j.cnsns.2014.02.022
14. Franović, K. Todorović, N. Vasović, N. Burić, Spontaneous formation of synchronization clusters in homogenous neuronal ensembles induced by noise and interaction delays, *Phys. Rev. Lett.*, **108** (2012), 094101. https://doi.org/10.1103/PhysRevLett.108.094101
15. S. Boccaletti, J. Kurths, G. Osipov, D. L. Valladares, C. S. Zhou, The synchronization of chaotic systems, *Phys. Rep.*, **366** (2002), 1–101. https://doi.org/10.1016/S0370-1573(02)00137-0
16. X. Li, P. K. Pal, Y. Lei, D. Ghosh, M. Small, Higher-order interactions induce stepwise explosive phase transitions, *Phys. Rev. E*, **111** (2025), 024303. https://doi.org/10.1103/PhysRevE.111.024303
17. R. Banerjee, S. Acharya, M. Perc, D. Ghosh, Anomalous complete synchronization in relay oscillators, *Chao Soliton. Fract.*, **193** (2025), 116069. https://doi.org/10.1016/j.chaos.2025.116069
18. X. Li, D. Ghosh, Y. Lei, M. Small, Synchronization and chimera states in time-varying multilayer networks with higher-order interactions, *Chaos*, **35** (2025). https://doi.org/10.1063/5.0258367
19. A. Arenas, A. D. Guilera, J. Kurths, Y. Moreno, C. Zhou, Synchronization in complex networks, *Phys. Rep.*, **469** (2008), 93–153. https://doi.org/10.1016/j.physrep.2008.09.002
20. C. Xu, X. Tang, H. Lü, K. A. Bittner, S. Boccaletti, M. Perc, Collective dynamics of heterogeneously and nonlinearly coupled phase oscillators, *Phys. Rev. Res.*, **3** (2021), 043004. https://doi.org/10.1103/PhysRevResearch.3.043004
21. E. Z. Serrano, J. M. M. Pacheco, A. A. Hernández, O. G. F. Beltrán, D. K. G. Flores, Synchronization of a cluster of β-cells based on a small-world network and its electronic experimental verification, *Eur. Phys. J.-Spec. Top.*, **231** (2022), 1035–1047. https://doi.org/10.1140/epjs/s11734-021-00307-6
22. A. Bashan, R. P. Bartsch, J. W. Kantelhardt, S. Havlin, P. Ch. Ivanov, Network physiology reveals relations between network topology and physiological function, *Nat. Commun.*, **3** (2012), 702. https://doi.org/10.1038/ncomms1705

23. J. Wan, G. Ichinose, M. Small, H. Sayama, Y. Moreno, C. Cheng, Multilayer networks with higher-order interaction reveal the impact of collective behavior on epidemic dynamics, *Chaos Soliton. Fract.*, **164** (2022), 112735. https://doi.org/10.1016/j.chaos.2022.112735
24. S. Ansarinasab, S. Panahi, F. Ghassemi, D. Ghosh, S. Jafari, Synchronization stability analysis of functional brain networks in boys with ADHD during facial emotions processing, *Physica A*, **603** (2022), 127848. https://doi.org/10.1016/j.physa.2022.127848
25. R. P. Bartsch, K. K. L. Liu, A. Bashan, A. Bashan, P. Ch. Ivanov, Network physiology: How organ systems dynamically interact, *PLoS One*, **10** (2015), e0142143. https://doi.org/10.1371/journal.pone.0142143
26. S. Eydam, I. Franović, L. Kang, Control of seizure-like dynamics in neuronal populations with excitability adaptation related to ketogenic diet, *Chaos*, **34** (2024). https://doi.org/10.1063/5.0180954
27. Y. Jia, H. Gu, Identifying nonlinear dynamics of brain functional networks of patients with schizophrenia by sample entropy, *Nonlinear Dynam.*, **96** (2019), 2327–2340. https://doi.org/10.1007/s11071-019-04924-8
28. X. Hu, Y. Wu, Q. Ding, W. Huang, Z. Ye, Y. Jia, et al., Inter-layer, intra-layer and complete synchronization in multiplex neuron networks, *Nonlinear Dynam.*, **113** (2025), 21813–21832. https://doi.org/10.1007/s11071-025-11266-1
29. L. M. Pecora, T. L. Carroll, Master stability functions for synchronized coupled systems, *Physi. Rev. Lett.*, **80** (1998), 2109–2112. https://doi.org/10.1103/PhysRevLett.80.2109
30. A. Nazerian, S. Panahi, F. Sorrentino, Synchronization in networks of coupled oscillators with mismatches, *Europhys. Lett.*, **143** (2023), 11001. https://doi.org/10.1209/0295-5075/acde5f
31. A. Nazerian, S. Panahi, F. Sorrentino, Synchronization in networked systems with large parameter heterogeneity, *Commun. Phys.*, **6** (2023), 253. https://doi.org/10.1038/s42005-023-01355-1
32. L. Huang, Q. Chen, Y. C. Lai, L. M. Pecora, Generic behavior of master-stability functions in coupled nonlinear dynamical systems, *Phys. Rev. E*, **80** (2009), 036204. https://doi.org/10.1103/PhysRevE.80.036204
33. J. W. Baron, Eigenvalue spectra and stability of directed complex networks, *Phys. Rev. E*, **106** (2022), 064302. https://doi.org/10.1103/PhysRevE.106.064302
34. M. Zarei, K. A. Samani, G. R. Omidi, Complex eigenvectors of network matrices give better insight into the community structure, *J. Stat. Mech.-Theory E.*, **2009** (2009), P10018. https://doi.org/10.1088/1742-5468/2009/10/P10018
35. Y. Sun, H. Zhao, J. Liang, X. Ma, Eigenvalue-based entropy in directed complex networks, *PLoS One*, **16** (2021), e0251993. https://doi.org/10.1371/journal.pone.0251993
36. I. Belykh, M. D. Bernardo, J. Kurths, M. Porfiri, Evolving dynamical networks, *Physica D*, **267** (2014), 1–6. https://doi.org/10.1016/j.physd.2013.10.008
37. S. Lin, X. Liu, Synchronization under control for fractional-order directed networks with multiweights, *J. Franklin I.*, **362** (2025), 107840. https://doi.org/10.1016/j.jfranklin.2025.107840
38. X. Deng, S. Ding, H. Lin, L. Jiang, H. Sun, J. Jin, Privacy-preserving online medical image exchange via hyperchaotic memristive neural networks and DNA encoding, *Neurocomputing*, **653** (2025), 131132. https://doi.org/10.1016/j.neucom.2025.131132
39. F. Yu, Y. Lin, W. Yao, S. Cai, H. Lin, Y. Li, Multiscroll Hopfield neural network with extreme multistability and its application in video encryption for IIoT, *Neural Networks*, **182** (2025), 106904. https://doi.org/10.1016/j.neunet.2024.106904

40. W. Yao, F. Yu, J. Zhang, L. Zhou, Asymptotic synchronization of memristive Cohen–Grossberg neural networks with time-varying delays via event-triggered control scheme, *Micromachines*, **13** (2022), 726. https://doi.org/10.3390/mi13050726
41. H. Shen, F. Yu, X. Kong, A. A. M. Mokbel, C. Wang, S. Cai, Dynamics study on the effect of memristive autapse distribution on Hopfield neural network, *Chaos*, **32** (2022), 083133. https://doi.org/10.1063/5.0099466
42. X. Kong, F. Yu, W. Yao, S. Cai, J. Zhang, H. Lin, Memristor-induced hyperchaos, multiscroll and extreme multistability in fractional-order HNN: Image encryption and FPGA implementation, *Neural Networks*, **171** (2024), 85–103. https://doi.org/10.1016/j.neunet.2023.12.008
43. F. Yu, X. Kong, W. Yao, J. Zhang, S. Cai, H. Lin, et al., Dynamics analysis, synchronization and FPGA implementation of multiscroll Hopfield neural networks with non-polynomial memristor, *Chaos Soliton. Fract.*, **179** (2024), 114440. https://doi.org/10.1016/j.chaos.2023.114440
44. L. Moysis, A. Tutueva, C. Volos, D. Butusov, J. M. M. Pacheco, H. Nistazakis, A two-parameter modified logistic map and its application to random bit generation, *Symmetry*, **12** (2020), 829. https://doi.org/10.3390/sym12050829
45. H. J. C. Mendoza, J. M. M. Pacheco, F. E. S. Moncada, R. T. Melendez, C. Volos, *A fractional order tumor growth model and its synchronization*, Proc. 2023 12th International Conference on Modern Circuits and Systems Technologies (MOCAST), 2023, 1–4. https://doi.org/10.1109/MOCAST57943.2023.10176372
46. V. Baysal, E. Erkan, E. Yilmaz, Impacts of autapse on chaotic resonance in single neurons and small-world neuronal networks, *Philos. T. Roy. Soc. A*, **379** (2021), 20200237. https://doi.org/10.1098/rsta.2020.0237
47. A. G. Korotkov, E. A. Grines, E. V. Syundyukova, E. V. Gubina, T. A. Levanova, Chaos in two heteroclinic cycles coupled with chemical synapses, *Eur. Phys. J.-Spec. Top.*, **234** (2025), 4009–4016. https://doi.org/10.1140/epjs/s11734-025-01723-8
48. N. V. Barabash, T. A. Levanova, L. A. Smirnov, Blue sky catastrophe in the phenomenological model of neuron–astrocyte interaction, *Chaos*, **34** (2024), 123141. https://doi.org/10.1063/5.0231551
49. V. Baysal, E. Yilmaz, Effects of electromagnetic induction on vibrational resonance in single neurons and neuronal networks, *Physica A*, **537** (2020), 122733. https://doi.org/10.1016/j.physa.2019.122733
50. S. Jafari, A. Bayani, F. Parastesh, K. Rajagopal, C. I. del Genio, L. Minati, et al., Periodic systems have new classes of synchronization stability, *Phys. Rev. Res.*, **6** (2024), 043105. https://doi.org/10.1103/PhysRevResearch.6.043105
51. L. F. Shampine, M. W. Reichelt, The MATLAB ODE suite, *SIAM J. Sci. Comput.*, **18** (1997), 1–22. https://doi.org/10.1137/S1064827594276424
52. Q. Xie, G. Chen, Synchronization stability analysis of the chaotic Rössler system, *Int. J. Bifurcat. Chaos*, **6** (1996), 2153–2161. https://doi.org/10.1142/S0218127496001429
53. S. K. Yang, C. L. Chen, H. T. Yau, Control of chaos in Lorenz system, *Chaos Soliton. Fract.*, **13** (2002), 767–780. https://doi.org/10.1016/S0960-0779(01)00052-2
54. R. Barrio, A. Shilnikov, Parameter-sweeping techniques for temporal dynamics of neuronal systems: case study of Hindmarsh–Rose model, *J. Math. Neurosci.*, **1** (2011), 6. https://doi.org/10.1186/2190-8567-1-6
55. S. Wiggins, Chaos in the quasiperiodically forced Duffing oscillator, *Phys. Lett. A*, **124** (1987), 138–142. https://doi.org/10.1016/0375-9601(87)90240-4

56. J. Guckenheimer, Dynamics of the Van der Pol equation, *IEEE T. Circ. Syst.*, **27** (1980), 983–989. https://doi.org/10.1109/TCS.1980.1084738
57. I. Prigogine, R. Lefever, Symmetry breaking instabilities in dissipative systems. II, *J. Chem. Phys.*, 48 (1968), 1695–1700. https://doi.org/10.1063/1.1668896
58. A. Bayani, F. Nazarimehr, S. Jafari, K. Kovalenko, G. C. Aso, K. A. Bittner, et al., The transition to synchronization of networked systems, *Nat. Commun.*, **15** (2024), 4955. https://doi.org/10.1038/s41467-024-48203-6
59. M. Lodi, F. D. Rossa, F. Sorrentino, M. Storace, Analyzing synchronized clusters in neuron networks, *Sci. Rep.*, **10** (2020), 16336. https://doi.org/10.1038/s41598-020-73269-9

AIMS Press

© 2026 the Author(s), licensee AIMS Press. This is an open access article distributed under the terms of the Creative Commons Attribution License (https://creativecommons.org/licenses/by/4.0)